43. Wei, X., Decker, J.M., Wang, S., Hui, H., Kappes, J.C., Wu, X., Salazar-Gonzalez, J.F., Salazar, M.G., Kilby, J.M., Saag, M.S., Komarova, N.L., Nowak, M.A., Hahn, B.H., Kwong, P.D. and Shaw, G.M., Antibody neutralization and escape by HIV-1. *Nature* 2003, **422:**307-312.

44. Weissenhorn, W., Hinz, A. and Gaudin, Y., Virus membrane fusion. *FEBS letters* 2007, **581:**2150-2155.

45. West, A.P., Jr., Galimidi, R.P., Gnanapragasam, P.N. and Bjorkman, P.J., Single-chain Fv-based anti-HIV proteins: potential and limitations. *J.Virol.* 2012, **86:**195-202.

46. White, J.M., Delos, S.E., Brecher, M. and Schornberg, K., Structures and mechanisms of viral membrane fusion proteins: multiple variations on a common theme. *Crit. Rev. Biochem. Mol. Biol.* 2008, **43:**189-219.

47. Wu, L., Gerard, N.P., Wyatt, R., Choe, H., Parolin, C., Ruffing, N., Borsetti, A., Cardoso, A.A., Desjardin, E., Newman, W., Gerard, C. and Sodroski, J., CD4-induced interaction of primary HIV-1 gp120 glycoproteins with the chemokine receptor CCR-5. *Nature* 1996, **384:**179-183.

FIGURE LEGENDS

Figure 1. Schematic diagram of pET28a3c-KD247-scFv. (A) The crystal structure of KD-247 F_{ab} (1.5 Å resolution, PDB: 3NTC) is shown with the complementarity determining regions (CDRs) highlighted in different colors. [Red: CDR 1 heavy chain (H1); Orange: CDR 2 heavy chain (H2); Purple: CDR 3 heavy chain (H3); Yellow: CDR 1 light chain (L1); Green: CDR 2 light chain (L2); Dark blue: CDR3 light chain (L3)]. The expected structure of KD-247 scFv was illustrated as a model. Figures were generated using PyMOL (8). (B) The variable domains of the heavy chain (V_H) and light chain (V_L) of KD-247 are connected with a peptide linker (L) to form the scFv. The twenty amino acid long peptide linker consists of four repeats of Glycine-Glycine-Glycine-Glycine-Serine, $(GGGGS)_4$. The scFv construct was subcloned at the N-terminal 6X Histidine tag (HIS_6) of the pET28a3c vector.

Figure 2. SDS-PAGE showing the optimization of KD-247 scFv overexpression in *E. coli*. (A) Overexpression of KD-247 scFv in Origami 2 (DE3) pLysS at various IPTG concentrations (0.25 mM,

0.5 mM, and 1 mM) were examined. (B) KD-247 scFv expression was induced at 37 °C or 30 °C. (C) Overexpression of KD-247 scFv in various *E. coli* strains was compared. As shown by the arrows, KD-247 scFv was expressed as inclusion bodies in *E. coli*. [Std: Protein standards; P: Pellet; S: Supernatant; B: Lysis Buffer]

Figure 3. Schematic representation of the purification and refolding of KD-247 scFv. KD-247 scFv was overexpressed in the BL21 (DE3) strain using the pET system. The pellet recovered after cell lysis was washed twice before denaturation with 6 M Gu-HCl containing β-mercaptoethanol. Denatured protein was refolded by first diluting in 6 M Urea and then dialyzing against 0.8 M Urea containing redox reagents cysteine and cystine. Partially refolded scFv was immobilized on a nickel column for further purification to remove residual urea. KD-247 scFv contains HIS_6 tag at the N-terminus, which enables nickel-affinity purification. scFvs eluted from the column were subjected to size-exclusion chromatography to obtain monomeric scFv.

Figure 4. Purification of KD-247 scFv from inclusion bodies. (A) SDS-PAGE showed proteins collected at various steps of purification. [P: pellet of lysed cells; S: supernatant of lysed cells; W1: supernatant after washing pellet with Wash Buffer A; W2: supernatant after washing pellet with Wash Buffer B; D: denatured scFv (diluted in 50 mM Tris-HCl pH 8.2, 150 mM NaCl)]. (B) Chromatogram showing the elution of scFvs from the nickel column. Blue line represents absorbance at 280 nm, red line represents absorbance at 254 nm. Elution fractions collected were analyzed by SDS-PAGE. (C) Size-exclusion chromatogram of KD-247 scFv in various refolded forms (blue solid line) compared to molecular weight standards (brown dashed line). Eluted scFvs in the monomeric fractions were analyzed by SDS-PAGE. (D) Native-PAGE of KD-247 F_{ab} compared to the monomeric KD-247 scFv recovered after concentration.

Figure 5. Far-UV circular dichroism (CD) spectra to evaluate secondary structures. The refolded KD-247 scFv (black) was compared to KD-247 F_{ab} (grey) in the absence of V3 peptide (A) and in the presence of V3 peptide (B). (C) CD of the refolded scFv at 25 °C (black), after 1 hour incubation at 37 °C (blue) and after overnight incubation at 37 °C (red).

TABLES

Table 1. Buffers for KD-247 scFv Purification

Lysis Buffer	50 mM Tris-HCl pH 8.2, 150 mM NaCl, 1 mM EDTA, 0.1% Triton X-100, 1 mM PMSF, 100 μg/ml lysozyme
Wash Buffer A	50 mM Tris-HCl pH 8.2, 150 mM NaCl, 3% Triton X-100, 1M Gu-HCl
Wash Buffer B	50 mM Tris-HCl pH 8.2, 150 mM NaCl
Denaturing Buffer	50 mM Tris-HCl pH 8.2, 150 mM NaCl, 6 M Gu-HCl, 10 mM β-mercaptoethanol
Refolding Buffer A	6 M Urea, 50 mM Tris-HCl pH 8.2, 150 mM NaCl
Refolding Buffer B	0.8 M Urea, 50 mM Tris-HCl pH 8.2, 150 mM NaCl, 2 mM Cysteine, 0.4 mM Cystine
Refolding Buffer C	50 mM Tris-HCl pH 8.2, 150 mM NaCl
Elution Buffer	50 mM Tris-HCl pH 8.2, 150 mM NaCl, 500 mM Imidazole

Table 2. 50% neutralizing activity (IC_{50}) of KD-247 scFv by TZM-bl cell assay

	Clade B HIV-1 Env		Clade C HIV-1 Env
	BaL	**JR-FL**	**ZM53M.PB12**
Maraviroc	0.001 μM	0.003 μM	0.003 μM
KD-247 Fab	0.1 μM	0.5 μM	> 5 μM
KD-247 scFv	0.2 μM	0.6 μM	> 5 μM

Type of file: figure
Label: Figure 1
Filename: Fig 1_Ong-01.tif

Fig. 1

(A)

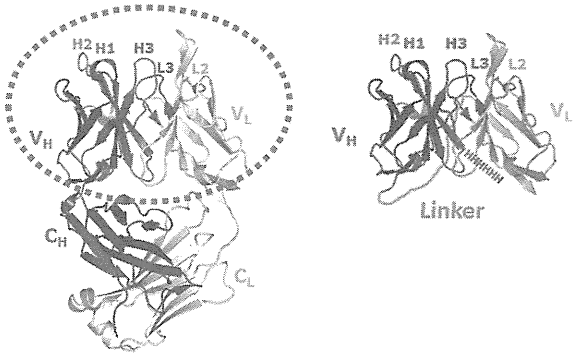
H2
H1
H3
L3
L2
V_H
V_L
C_H
C_L
Linker

(B)

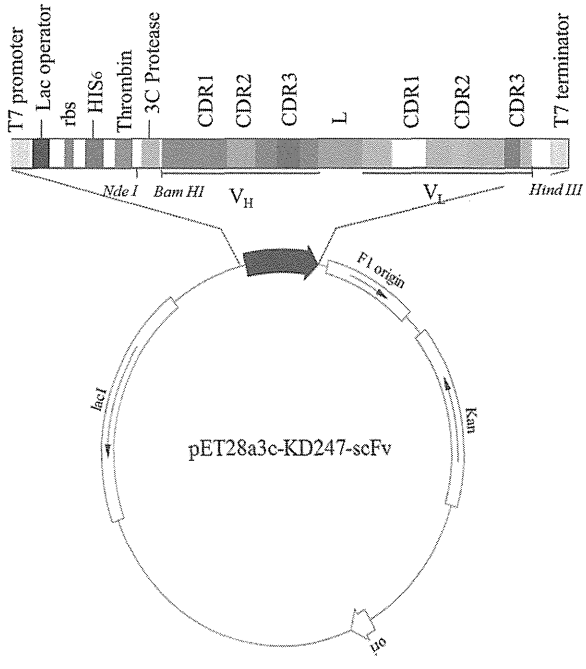
T7 promoter
Lac operator
rbs
HIS6
Thrombin
3C Protease
CDR1
CDR2
CDR3
L
CDR1
CDR2
CDR3
T7 terminator
Nde I
Bam HI
V_H
V_L
Hind III
F1 origin
lacI
Kan
pET28a3c-KD247-scFv
ori

Type of file: figure
Label: Figure 2
Filename: Fig 2_Ong-01.tif

Fig. 2

(A)

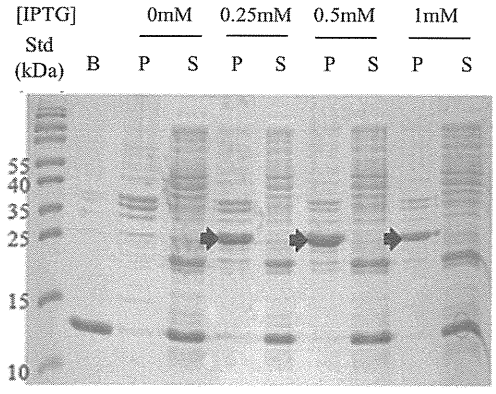
[IPTG]
0mM
0.25mM
0.5mM
1mM
Std (kDa)
B
P
S
P
S
P
S
P
S
55
40
35
25
15
10

(B)

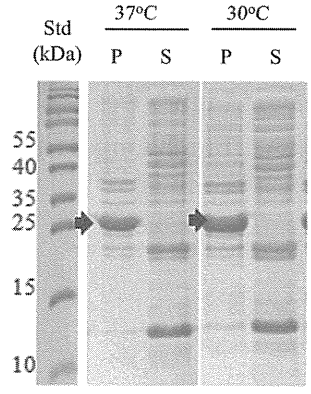
Std (kDa)
37°C
30°C
P
S
P
S
55
40
35
25
15
10

(C)

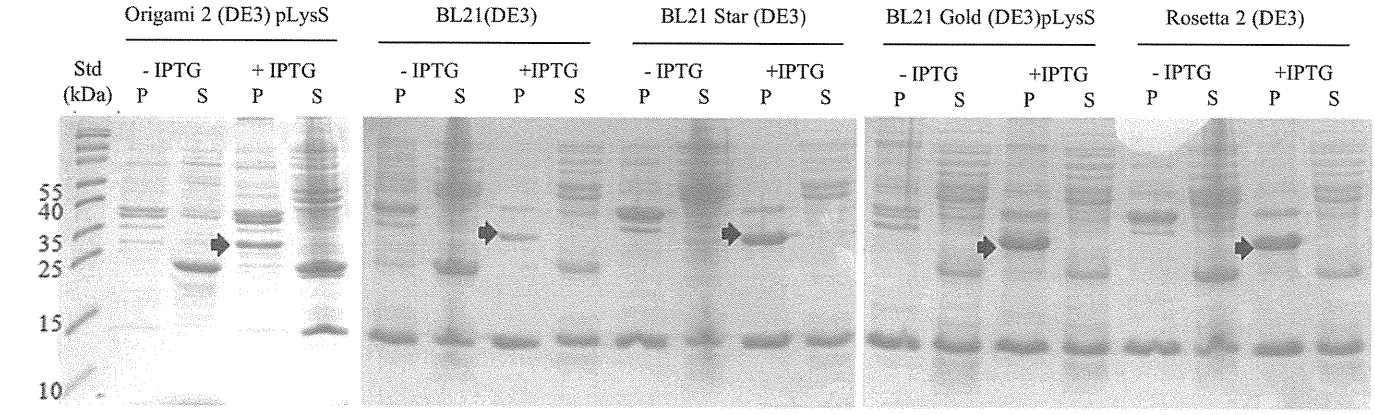
Origami 2 (DE3) pLysS
BL21(DE3)
BL21 Star (DE3)
BL21 Gold (DE3)pLysS
Rosetta 2 (DE3)
Std (kDa)
- IPTG
+ IPTG
P
S
55
40
35
25
15
10

Type of file: figure
Label: Figure 3
Filename: Fig 3_Ong-01.tif

Fig. 3

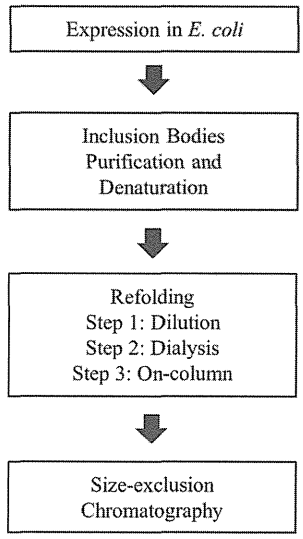
Expression in E. coli
Inclusion Bodies
Purification and
Denaturation
Refolding
Step 1: Dilution
Step 2: Dialysis
Step 3: On-column
Size-exclusion
Chromatography

Type of file: figure
Label: Figure 4
Filename: Fig 4_Ong-01.tif

Fig. 4

(A)

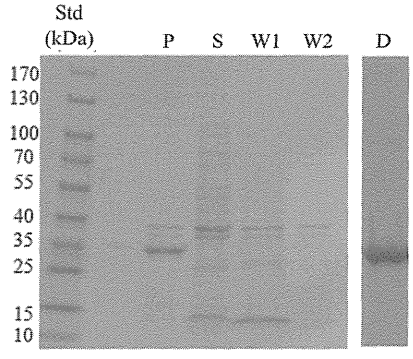
Std
(kDa)
P
S
W1
W2
D
170
130
100
70
55
40
35
25
15
10

(D)

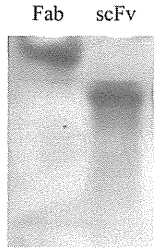
Fab
scFv

(B)

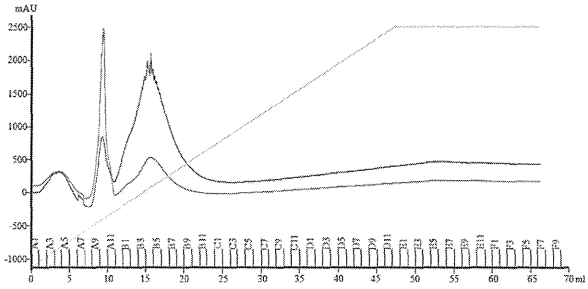
mAU
ml

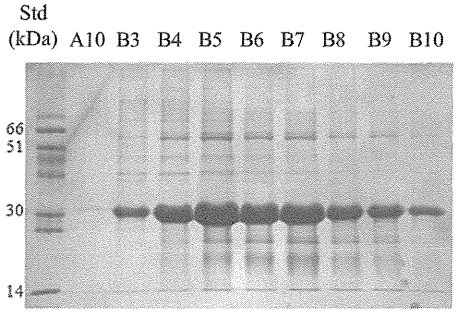
Std
(kDa)
A10
B3
B4
B5
B6
B7
B8
B9
B10
66
51
30
14

(C)

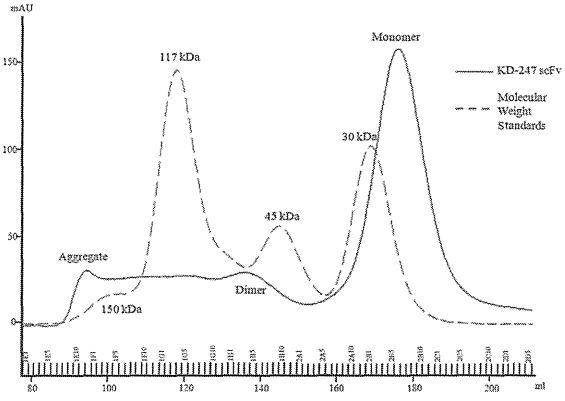
mAU
117 kDa
Monomer
KD-247 scFv
Molecular
Weight
Standards
30 kDa
45 kDa
Aggregate
Dimer
150 kDa
ml

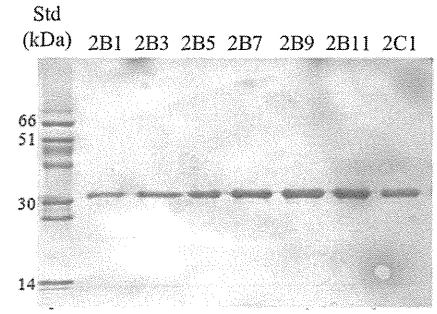
Std
(kDa)
2B1
2B3
2B5
2B7
2B9
2B11
2C1
66
51
30
14

Type of file: figure
Label: Figure 5
Filename: Fig 5_Ong-01.tif

Fig. 5

(A)

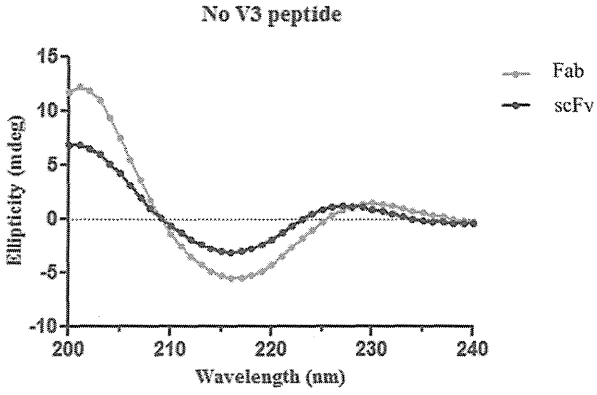
No V3 peptide
Ellipticity (mdeg)
15
10
5
0
-5
-10
200
210
220
230
240
Wavelength (nm)
Fab
scFv

(B)

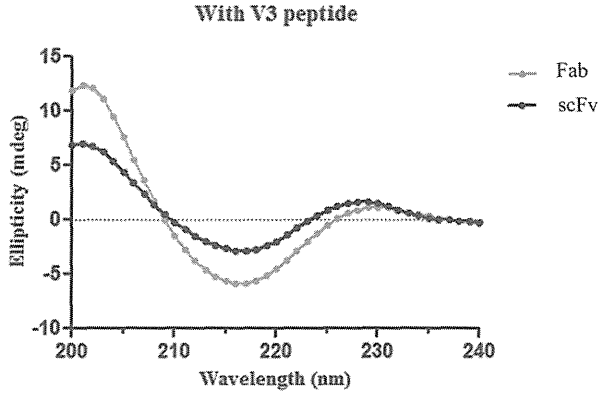
With V3 peptide
Ellipticity (mdeg)
15
10
5
0
-5
-10
200
210
220
230
240
Wavelength (nm)
Fab
scFv

(C)

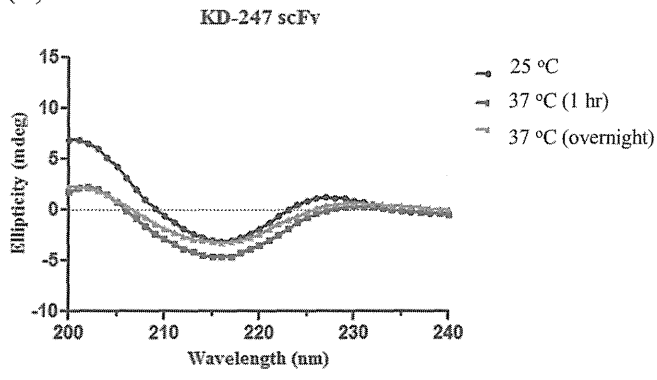
KD-247 scFv
Ellipticity (mdeg)
15
10
5
0
-5
-10
200
210
220
230
240
Wavelength (nm)
25 °C
37 °C (1 hr)
37 °C (overnight)

OPEN ACCESS Freely available online

PLoS one

Structural Dynamics of HIV-1 Envelope Gp120 Outer Domain with V3 Loop

Masaru Yokoyama[1]*, Satoshi Naganawa[2], Kazuhisa Yoshimura[3], Shuzo Matsushita[3], Hironori Sato[1]*

1 Laboratory of Viral Genomics, Pathogen Genomics Center, National Institute of Infectious Diseases, 4-7-1 Gakuen, Musashi Murayama-shi, Tokyo, Japan, **2** Department of Microbiology and Cell Biology, Tokyo Metropolitan Institute of Medical Science, 2-1-6 Kamikitazawa, Setagaya-ku, Tokyo, Japan, **3** Division of Clinical Retrovirology and Infectious Diseases, Center for AIDS Research, Kumamoto University, 2-2-1 Honjo, Kumamoto, Japan

Abstract

Background: The net charge of the hypervariable V3 loop on the HIV-1 envelope gp120 outer domain plays a key role in modulating viral phenotype. However, the molecular mechanisms underlying the modulation remain poorly understood.

Methodology/Principal Findings: By combining computational and experimental approaches, we examined how V3 net charge could influence the phenotype of the gp120 interaction surface. Molecular dynamics simulations of the identical gp120 outer domain, carrying a V3 loop with net charge of +3 or +7, showed that the V3 change alone could induce global changes in fluctuation and conformation of the loops involved in binding to CD4, coreceptor and antibodies. A neutralization study using the V3 recombinant HIV-1 infectious clones showed that the virus carrying the gp120 with +3 V3, but not with +7 V3, was resistant to neutralization by anti-CD4 binding site monoclonal antibodies. An information entropy study shows that otherwise variable surface of the gp120 outer domain, such as V3 and a region around the CD4 binding loop, are less heterogeneous in the gp120 subpopulation with +3 V3.

Conclusions/Significance: These results suggest that the HIV-1 gp120 V3 loop acts as an electrostatic modulator that influences the global structure and diversity of the interaction surface of the gp120 outer domain. Our findings will provide a novel structural basis to understand how HIV-1 adjusts relative replication fitness by V3 mutations.

Citation: Yokoyama M, Naganawa S, Yoshimura K, Matsushita S, Sato H (2012) Structural Dynamics of HIV-1 Envelope Gp120 Outer Domain with V3 Loop. PLoS ONE 7(5): e37530. doi:10.1371/journal.pone.0037530

Editor: John J. Rossi, Beckman Research Institute of the City of Hope, United States of America

Received February 21, 2012; **Accepted** April 20, 2012; **Published** May 18, 2012

Funding: This work was supported by grants-in-aid from the Ministry of Health, Labor and Welfare, Japan. The funders had no role in study design, data collection and analysis, decision to publish, or preparation of the manuscript.

Competing Interests: The authors have declared that no competing interests exist.

* E-mail: yokoyama@nih.go.jp (MY); hirosato@nih.go.jp (HS)

Introduction

The third variable (V3) element of the human immunodeficiency virus type 1 (HIV-1) envelope gp120 protein is usually composed of 35 amino acids. The element forms a protruding loop-like structure on the gp120 outer domain [1], is rich in basic amino acids, and has aromatic amino acids for the aromatic stacking interaction with proteins. The V3 loop participates in direct binding to the entry coreceptor [2] and constitutes the most critical determinant for the coreceptor use of HIV-1 [3,4,5,6]. In addition, the tip of V3 is highly immunogenic and contains neutralization epitopes for antibodies [7,8,9], although the epitopes can be inaccesible in the gp120 trimer on a virion of the HIV-1 primary isolates [10,11] or HIV-1 recombinants with less positively charged V3 [12,13]. Moreover, the V3 is reported to be the major determinant of HIV-1 sensitivity to neutralization by the soluble form of CD4 [14,15,16], a recombinant protein that binds to the cleft of the gp120 core [17]. Thus, the V3 loop plays a key role in modulating biological and immunological phenotypes of HIV-1. However, the molecular mechanisms underlying these modulations remain poorly understood.

It has been reported that the net charge of the V3 loop is tightly linked to the phenotype of HIV-1. The V3 loops of CCR5 tropic HIV-1s are usually less positively charged than those of CXCR4 tropic HIV-1s [18,19,20,21]. An increase in the V3 net charge can convert CCR5 tropic viruses into CXCR4 tropic viruses [4,22,23,24], and antibody resistant viruses into sensitive viruses [12,13]. Thus the V3 loop may be viewed as an electrostatic modulator of the structure of the gp120 interaction surface, an assumption that is largely unexamined.

Increasing evidence has indicated that the dynamics property of molecules in solution is critical for protein function and thus for many biological processes [25,26,27]. Molecular dynamic (MD) simulation is a powerful method that predicts the structural dynamics of biological molecules in solution, which is often difficult to analyze by experiments alone [28,29,30]. Recent advances in biomolecular simulation have rapidly improved the precision and application performance of this technique [28,29,30]. We have previously applied this technique to investigating the structural factors that regulate biological phenotype of viruses [13,31,32]. In this study, by combining MD simulations with antibody neutralization experiments and diversity analysis of the viral protein sequences, we studied a structural basis for the regulation of HIV-1 phenotype by V3 loop.

Results

Molecular dynamics simulation study

To address the potential role of the V3 net charge in modulating the structure and dynamics of the gp120 surface, we performed MD simulations of the identical gp120 outer domains carrying different V3 loops with net charges of +7 or +3 (Fig. 1A). The initial structures for the simulations were constructed by homology modeling using the crystal structure of HIV-1 gp120 containing an entire V3 loop as the template. Due to the perfect identity of the outer domain sequences of the V3 recombinant gp120s, the outer domain structures of the initial models for the MD simulations were identical before the simulations. The modeling targets in this study belong to HIV-1 subtype B and had a sequence similarity of about 87.3% to the modeling template. This similarity was high enough to construct high-accuracy models with an RMSD of ~1.5 Å for the main chain between the predicted and actual structures in the tested cases with homology models and x-ray crystal structures [33]. These initial models were lacking in V1/V2 loops and glycans on the gp120. The recombinant models are therefore suitable for exploring the potency of the structural regulation that is intrinsic to the V3 loop.

Using these models as the initial structures, we analyzed the structural dynamics of the gp120 outer domains in the absence of soluble CD4 by MD simulation. It was expected that the MD simulations would eliminate initial distortions in the template crystal structure, which could be generated during crystallization, and search for the most stable structures of unliganded gp120 outer domains at 1 atm at 310 K in water. The simulations showed that the same gp120 outer domains, carrying different V3 loops with net charges of +7 or +3, exhibited marked changes in conformations and fluctuations at several functional loops at 1 atm at 310 K in water (Figs. 1 and 2).

To quantitatively monitor the overall structural dynamics of the outer domain during MD simulation, the RMSDs between the initial model and models at given times of MD simulation were measured. The RMSD sharply increased soon after heating of the initial model and then gradually reached a near plateau after 10 ns of the MD simulations (Fig. 1B). The results suggested that most of the backbone heavy atoms of the outer domain reached a thermodynamic equilibrium after 10 ns of the simulation under the conditions employed. However, fluctuations of the RMSDs were still detectable even at around 30 ns of the simulations, suggesting that some regions of the outer domains continued to fluctuate.

To map the heavily fluctuating sites in the gp120 outer domain, we calculated the RMSF of the main chains of individual amino acids during the MD simulations. The RMSFs, which provide information about the atomic fluctuations during MD simulations [34], were found to be much greater in the amino acids constituting loops than those of the structured regions, such as helixes and β-sheets (Figs. 1C and 1D). These results are consistent with the general observations of proteins in solution, and indicate that the loops of the gp120 outer domain intrinsically possess structural flexibility in water. Notably, the RMSFs in some loops were markedly different between the two V3 recombinant gp120s. For example, the RMSF in the β20–β21 loop was much greater in the $Gp120_{LAI\text{-}TH09V3}$ (Fig. 1C). Conversely, those in the D loop were greater in the $Gp120_{LAI\text{-}NH1V3}$.

HIV-1 gp120 V3 loop often has a motif for the N-linked glycosylation that is usually preferentially conserved in R5 viruses (Fig. 1A). To address potential impacts of the glycan on the MD simulations, we performed MD simulation in the presence of a high mannose oligosaccharide in the V3 loop. We observed any significant differences in the structure and dynamics of gp120 outer domain in the presence or absence of the glycan (data not shown). This is reasonable because the glycosylation site is exposed toward an opposite direction from the gp120 core (Fig. 1D).

To clarify structural differences between the $Gp120_{LAI\text{-}NH1V3}$ and $Gp120_{LAI\text{-}TH09V3}$, we constructed their averaged structures using the 40,000 snapshots obtained from 10–30 ns of MD simulations using ptraj module in Amber 9. Superposition of the averaged structures showed that the relative configuration of the V3 loops and β20–β21 was markedly different between the two outer domains: the V3 tip protruded a greater distance from the β20–β21 loop in the $Gp120_{LAI\text{-}TH09V3}$ than in the $Gp120_{LAI\text{-}NH1V3}$ (Fig. 2A). The superposed structures also revealed differences in a region around the CD4 binding site (Fig. 2A, right panel with enlarged CD4 binding site). The relative configuration of the CD4 binding loop to the exit loop is critical for the gp120 binding to the CD4, a primary infection receptor of HIV-1 [17]. Therefore, we analyzed the distance between the CD4 binding and exit loops by measuring the distance ($D_{115\text{–}221}$) between the Cα of Gly115 and the Cα of Gly221 as an indicator (Fig. 2B). As expected from the fluctuations of the CD4 binding loop, the $D_{115\text{–}221}$ fluctuated during the MD simulations (Fig. 2C). However, the $D_{115\text{–}221}$ was significantly smaller in the $Gp120_{LAI\text{-}TH09V3}$ than in the $Gp120_{LAI\text{-}NH1V3}$ (Fig. 2D; $p<0.001$, Student's *t*-test): the $D_{115\text{–}221}$ ranged from 4–15 Å with an average of ~8 Å for the $Gp120_{LAI\text{-}TH09V3}$ and from 7–17 Å with an average of ~10 Å for the $Gp120_{LAI\text{-}NH1V3}$. These data suggest that the CD4 binding loop tended to be positioned more closely to the exit loop and thus tended to be sterically less exposed in the $Gp120_{LAI\text{-}TH09V3}$ than the $Gp120_{LAI\text{-}NH1V3}$.

Neutralization study

The above structural data raised the possibility that the reduction in the V3 net charge might reduce HIV-1 neutralization sensitivity by the anti-CD4 binding site antibodies. To address this possibility, we performed a neutralization assay using the two isogenic HIV-1 recombinant viruses, $HIV\text{-}1_{LAI\text{-}NH1V3}$ and $HIV\text{-}1_{LAI\text{-}TH09V3}$ [35], which carry the $Gp120_{LAI\text{-}NH1V3}$ and $Gp120_{LAI\text{-}TH09V3}$, respectively. These viruses were pre-incubated with various human MAbs against the CD4 binding site, and the reductions in viral infectious titers were measured using a HeLa-cell-based single-round viral infectivity assay system [36].

Table 1 summarizes the results of the neutralization assay. As expected, the two viruses exhibited markedly distinct neutralization sensitivities to the three human MAbs against the CD4 binding site. $HIV\text{-}1_{LAI\text{-}NH1V3}$ was consistently neutralized with all three MAbs against the CD4 binding site (49G2, 42F6, and 0.5δ), with ND_{50} values ranging between 0.224 and 0.934 μg/ml. In marked contrast, $HIV\text{-}1_{LAI\text{-}TH09V3}$ was highly resistant to neutralization by these MAbs, and 10 μg/ml of antibodies failed to block the viral infections. The two viruses were equally resistant to an anti-Gp120 antibody (4C11) that recognizes the Gp120 structure after CD4 binding. The result indicates that the CD4-induced gp120 epitope of the 4C11 are not preserved in the V3 recombinant viruses used in the present study. Conversely, they were equally sensitive to another ant-Gp120 antibody (4301 [37]) whose epitope is located outside of the CD4 binding site. A human MAb 8D11 used as a negative control had no effect on the viral infectivity in this assay.

Diversity study

Host immunity is a driving force behind the antigenic diversity of envelope proteins of the primate lentiviruses that establish persistent infection in hosts [23,38,39,40,41]. The above and

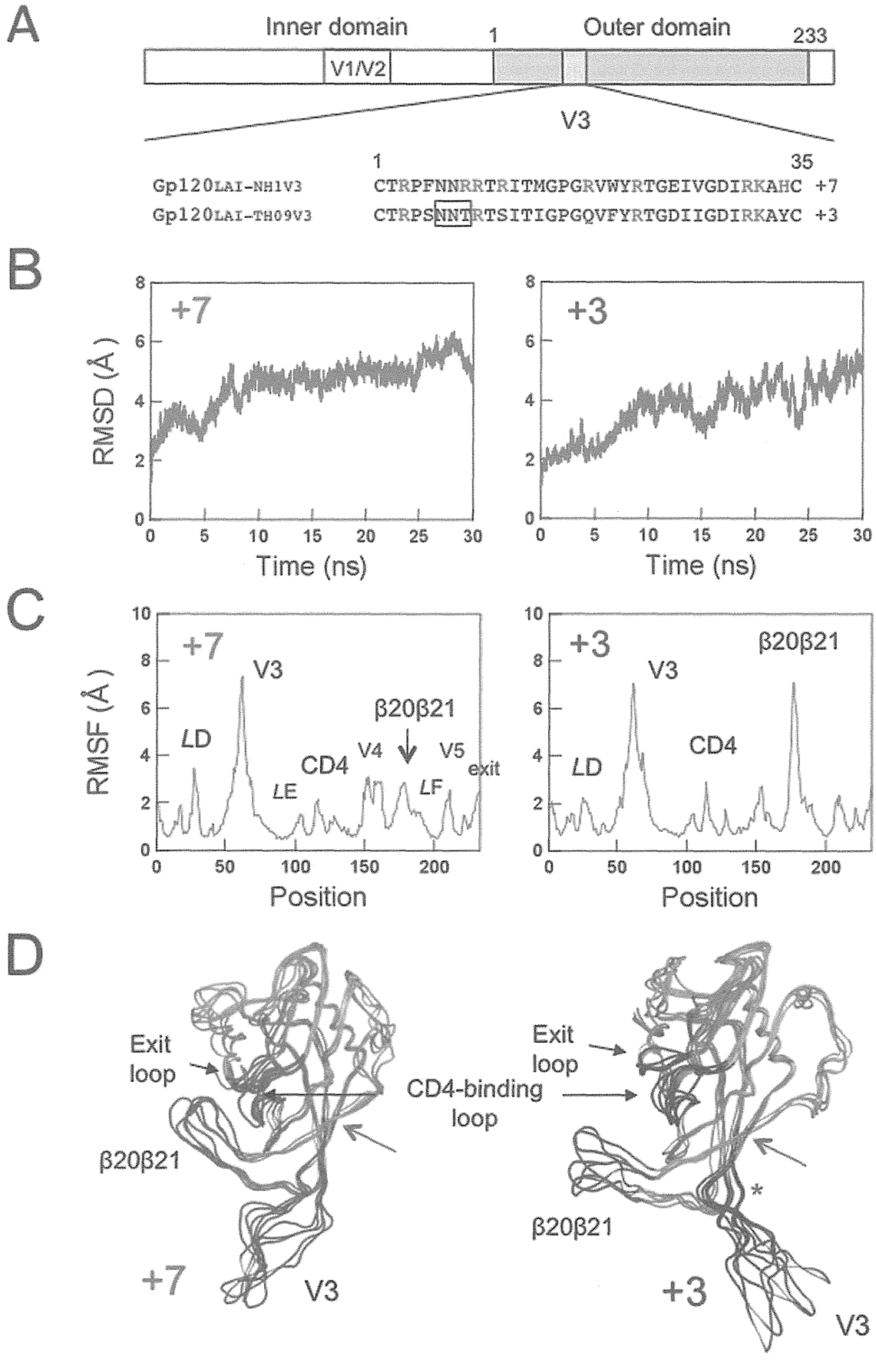
A
Inner domain
1
Outer domain
233
V1/V2
V3
1
35
Gp120LAI-NH1V3 CTRPFNNRRTRITMGPGRVWYRTGEIVGDIRKAHC +7
Gp120LAI-TH09V3 CTRPSNNTRTSITIGPGQVFYRTGDIIGDIRKAYC +3
B
+7
+3
RMSD (Å)
Time (ns)
C
+7
+3
V3
β20β21
LD
CD4
V4
V5
exit
LE
LF
RMSF (Å)
Position
D
Exit loop
CD4-binding loop
β20β21
+7
+3
V3
*

Figure 1. MD simulation of the identical gp120 outer domain carrying a V3 loop with net charge of +7 or +3. (A) Schematic representation of the gp120 open reading frame along with the amino acid sequences. The net charge indicates the number of positively charged amino acids (R, K, and H) minus the number of negatively charged amino acids (D and E) in the V3 loop. A light blue box indicates the outer domain used for the MD simulations. A pink box indicates the V3 loop. The numbers indicate amino acid positions at the outer domain (amino acids 1 to 233 in Figure 1A correspond to amino acids 256 to 489 in the gp120 of HIV-1_{LAI}) or the V3 loop. An open black box in the V3 loop sequence indicates a potential site for the N-linked glycosylation. (B–D) Left panels: $Gp120_{LAI\text{-}NH1V3}$; Right panels: $Gp120_{LAI\text{-}TH09V3}$. +7 and +3 indicate the net charges of V3 loops of the recombinant proteins. (B) Time course of RMSD during MD simulations. The RMSD values indicate the structural fluctuations of the outer domain in aqueous solution. The numbers in the horizontal axes indicate the time of MD simulation. (C) Distribution of RMSF in the gp120 outer domain. The RMSF values indicate the atomic fluctuations of the main chains of individual amino acids during 10–30 ns of MD simulations. The numbers in the horizontal axes indicate amino acid positions at the outer domain. (D) Superimposition of Gp120 models at 10, 15, 20, 25, and 30 ns of MD simulation. A green asterisk indicates approximate position of a potential N-glycosylation site at the V3 stem. A green arrow indicates the site of the disulfide bond at the V3 base.
doi:10.1371/journal.pone.0037530.g001

previous [12,13,14,15,16] neutralization studies raised the possibility that the gp120 surface might be less heterogeneous in gp120 subpopulations that have a less positively charged V3 loop, due to greater magnitudes of resistance to the antibody neutralization. To address this possibility, we performed an information entropy study using sequences in the public database. We extracted full-length gp120 amino acid sequences of HIV-1 subtype CRF01_AE that has the same evolutionary origin and is spread throughout southeast Asia [42]), and divided them into subgroups on the basis of the net charge of V3 loop (+2, +3, +4, +5, +6, +7, and +8). The sequences were used to calculate the Shannon entropy scores, *H(i)* [1], to denote the diversity of individual amino acids within each subpopulation.

Figure 3 shows the 3-D distribution of the *H(i)* scores of individual amino acids plotted on the HIV-1 gp120 crystal structure (PDB code: 2B4C [1]), where the green to orange regions were suggested to have more variable amino acids than the blue ones. In the gp120 subpopulation that has +7 V3 loop, the *H(i)* scores often exceeded 2.0 bits at many residues, reaching close to the maximum value of 4.4, i.e., the diversity was maximal, at the V5 region (Fig. 3A, left panel). Regions with high *H(i)* scores included the functional sites, such as the V3 loop and the regions around the CD4 binding site. In marked contrast, in the gp120 subpopulation carrying the +3 V3 loop, the *H(i)* scores were almost zero, i.e., the diversity was minimal, at many amino acids, but not at those in the V4, V5, and *LE* regions (Fig. 3A, right panel). Importantly, relatively high levels of conservation were also detected with amino acids in the otherwise highly variable V3 loop. Moreover, a region adjacent to the CD4 binding loop was also less heterogeneous compared with those of the gp120 subpopulation carrying +7 V3 loop (Figs. 3B). In the gp120 subpopulations carrying the +2, +3, 4, and +5 V3 loops, the *H(i)* scores were indistinguishable from each other: they were less heterogeneous than the subpopulations carrying the +6, +7, and +8 V3 loops. Similar results were obtained with HIV-1 subtype C that represents the most predominated HIV-1 in the world (data not shown).

Discussion

The ability of HIV-1 to rapidly change its phenotype greatly complicates our efforts to eradicate this virus. Elucidation of structural principles for the phenotypic change may provide a clue to control HIV-1. In this study, by combining MD simulations with antibody neutralization experiments and diversity analysis of the viral protein sequences, we studied a structural basis for the phenotypic change of HIV-1 by V3 mutations. To address this issue, we used a V3 recombinant system; we performed a computer-assisted structural study and an infection-based neutralization assay using gp120 proteins whose amino acid sequences are identical except for V3 loop. In combination with an informatics study, we obtained evidence that the HIV-1 V3 loop acts as an electrostatic modulator that influences the global structure and diversity of the interaction surface of the gp120 outer domain.

Using MD simulation, we first examined whether the V3 net charge could affect the structural dynamics of the HIV-1 gp120 outer domain surface. Initial structures of the outer domain of the two gp120s, $Gp120_{LAI\text{-}NH1V3}$ and $Gp120_{LAI\text{-}TH09V3}$, were identical before MD simulations, because the domains were both derived from HIV-1_{LAI} strain. Remarkably, however, the two molecules with distinct V3 loop exhibited markedly distinct structural dynamics following MD simulations (Figs. 1 and 2). These data strongly suggest that the V3 net charge can act as an intrinsic modulator that influences the structural dynamics of the interaction surface of the gp120 outer domain. Such a global effect on structure by a local electrostatic change has been reported with bacteriorhodopsin [43]. In general, the long-range effects of non-electrostatic contributions are negligible, whereas those of the electrostatic contributions are not [34]. Therefore, it is reasonable that the changes in overall charge of the V3 loop element caused the global effects on the gp120 structure via alteration of the electrostatic potentials of the gp120 surface.

We next studied biological impact of the structural changes predicted by MD simulations. The MD simulations suggested that the CD4 binding loop was less exposed in the $Gp120_{LAI\text{-}NH1V3}$ than the $Gp120_{LAI\text{-}NH1V3}$ (Fig. 2). The finding predicted that reduction in V3 net charge could cause reduction in neutralization sensitivity to the anti-CD4 binding site antibodies. This possibility was assessed by neutralization assay. We used infectious HIV-1_{LAI} clones having the $Gp120_{LAI\text{-}NH1V3}$ or the $Gp120_{LAI\text{-}TH09V3}$ to assess their neutralization sensitivities to the anti-CD4 binding site MAbs. Notably, we indeed observed marked reduction in the neutralization sensitivity in HIV-1_{LAI} having $Gp120_{LAI\text{-}TH09V3}$ (Table 1). The results are consistent with the structural changes predicted by MD simulations, as well as previous findings on neutralization sensitivity of HIV-1s to soluble CD4 [14,15,16].

We further studied evolutionary impact predicted by MD simulations and the neutralization studies. These studies predicted that reduction in V3 net charge could cause reduction in sequence diversity around the CD4 binding site due to reduced sensitivity to positive selection pressures of antibodies. Notably, we indeed observed marked reduction in the gp120 diversity: our Shannon entropy data show that otherwise variable surfaces of gp120, such as V3 and a region around the CD4 binding loop, are less heterogeneous in the gp120 subgroups carrying a V3 loop with a +3 charge (Fig. 3).

Previous cryo-electron microscopy studies have indicated that gp120 forms a trimer on an HIV-1 virion, where the CD4 binding sites are exposed on the outside surface in the solution [44,45,46]. Therefore, it is reasonable that gp120 with +3 V3 with less exposed CD4 binding loop is less sensitive to neutralization by anti-CD4 binding site antibodies (Table 1) and less heterogeneous around the CD4 binding site (Fig. 3). Collectively, our results

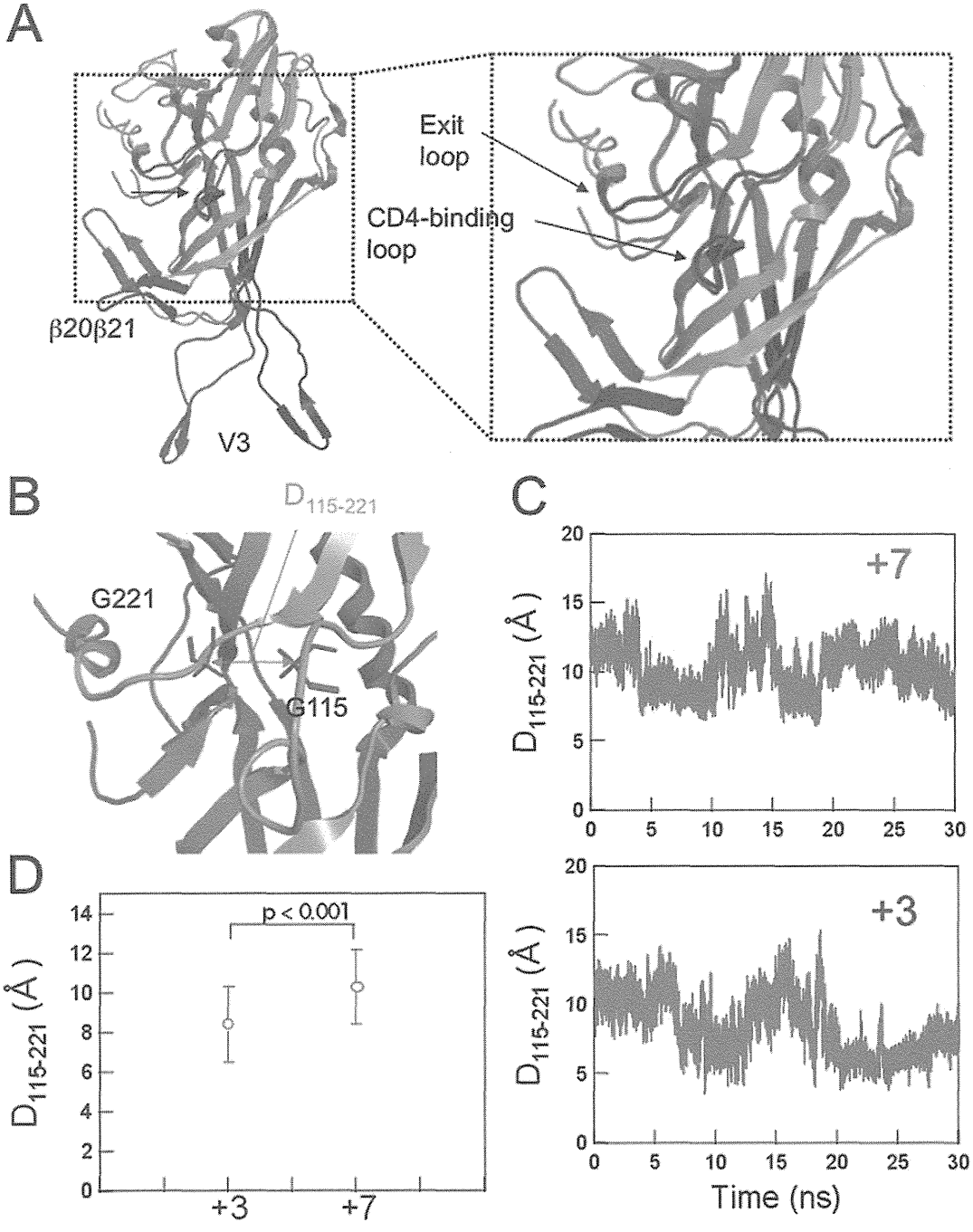

Figure 2. Comparison of the averaged 3-D models during MD simulation. (A) Superposition of the averaged structures obtained with the 40,000 snapshots obtained from 10–30 ns of MD simulations using ptraj module in Amber 9. Red and Blue ribbons: loops of $Gp120_{LAI\text{-}NH1V3}$ and $Gp120_{LAI\text{-}TH09V3}$ with V3 net charges of +7 and +3, respectively. (B–D) Configuration and structural dynamics of the CD4 binding loop. The distance between the Cα of Gly115 and the Cα of Gly221 in the CD4 binding loop was calculated to monitor configurational changes (B). The distance was monitored during the 10–30 ns of MD simulation (C) and the average distance with variance was plotted (D). +7: $Gp120_{LAI\text{-}NH1V3}$; +3: $Gp120_{LAI\text{-}TH09V3}$.
doi:10.1371/journal.pone.0037530.g002

obtained with all three approaches agree with each other and suggest that V3 net charge is an intrinsic factor that influences structural property, antibody sensitivity, and sequence diversity of CD4 binding site.

The HIV-1 gp120 outer domain has several functional or immunogenic loops involved in binding to CD4, coreceptor and antibodies. Our MD simulations predicted that V3 net charge influences fluctuation and conformation of these loops (Figs. 1 and 2). The V3-based structural modulation of the gp120 surface loops may be an effective mechanism to alter effectively the phenotype and relative fitness of HIV-1. For example, a change in the V3 net charge by mutations may induce changes in V3 conformation (Figs. 1D and 2A) [13], which in turn may influence intra- or intermolecular interactions among gp120 monomers and thus global structure of gp120 trimer on a virion. Generation of a swarm of structural variants by V3 mutations could help generating the best-

Table 1. Neutralization sensitivity of the isogenic V3 recombinant HIV-1 to anti-gp120 monoclonal antibodies.

Antibody ID	Ig subtype	Epitopes on Gp120	ND_{50} (μg/ml)[@]	
			$HIV\text{-}1_{LAI\text{-}NH1V3}$	$HIV\text{-}1_{LAI\text{-}TH09V3}$
49G2	human IgG1	CD4 binding site[#]	0.224	>10
42F9	human IgG1	CD4 binding site[#]	0.934	>10
0.5δ [59]	human IgG1	CD4 binding site[#]	0.444	>10
4C11 [59]	human IgG2	CD4 induced structure[$]	>20	>10
4301	mouse IgG	broadly reactive*	0.59	0.57
8D11	human IgG1	none	>20	>10

[#]Neutralization epitope in the Gp120 outer domain before CD4 binding.
[$]Neutralization epitope induced in Gp120 after CD4 binding.
*Epitopes outside of the CD4 binding site [37].
[@]The effect of each antibody on viral infectivity was tested in duplicate.
doi:10.1371/journal.pone.0037530.t001

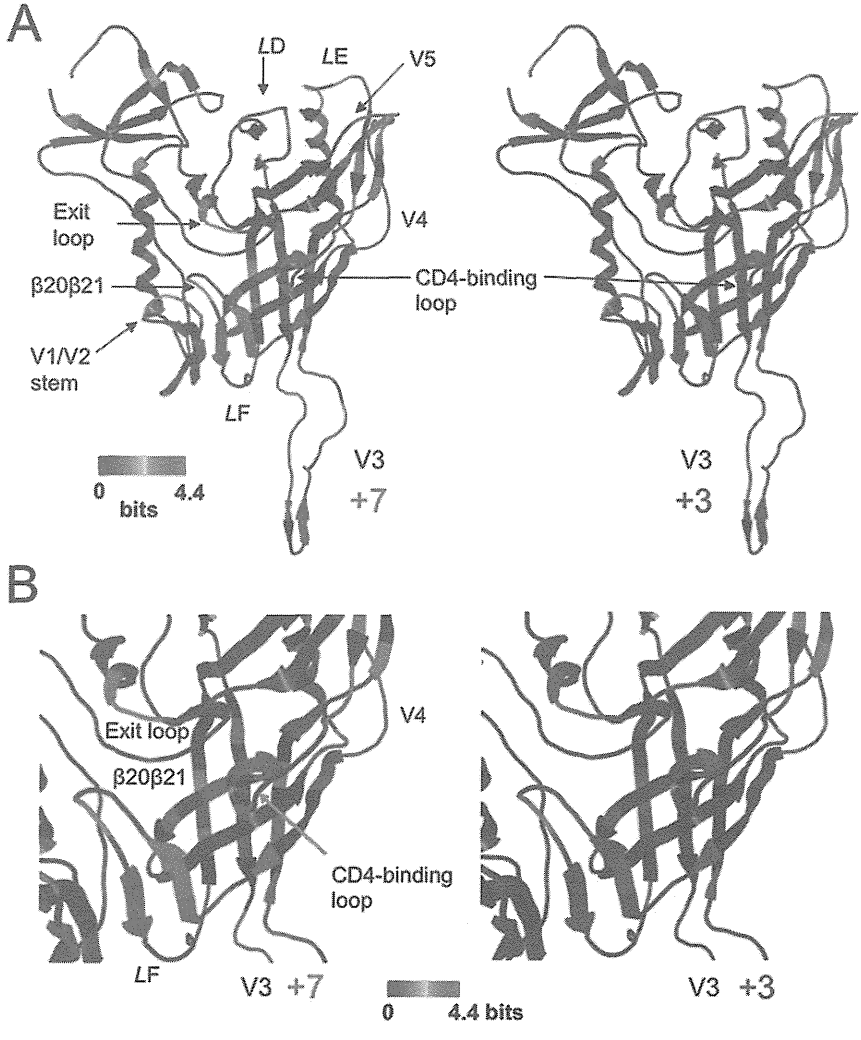

Figure 3. Diversity of the gp120 subpopulations carrying a V3 loop with net charge of +7 or +3. Full-length gp120 sequences of the HIV-1 CRF01_AE [42] were extracted from a public database, and divided into subgroups on the basis of the net charge of the V3 loop (+2~+8). The divided sequences were used to calculate the Shannon entropy, *H(i)* [63], within each subpopulation, and the *H(i)* values were plotted on the 3-D structure of gp120 (PDB code: 2B4C [1]). The results for the gp120 subgroups that have V3 loops with +7 (left panel) and +3 (right panel) charges are shown as representative. The numbers of sequences used to calculate the *H(i)* were 9 and 81 for +7 and +3, respectively. (A) Distribution of *H(i)* in the gp120 monomer. (B) Distribution of *H(i)* around the CD4 binding site.
doi:10.1371/journal.pone.0037530.g003